An integrated multi-omics study to identify dynamic molecular alterations associated with acute brain injury

Shigang Yin (✉ sgyin@swmu.edu.cn)
Southwest Medical University https://orcid.org/0000-0003-0955-917X
Yong Jiang (✉ jiangyong@swmu.edu.cn)
Southwest Medical University https://orcid.org/0000-0002-0490-3405
Jianhua Peng (✉ pengjianhua@swmu.edu.cn)
Southwest Medical University https://orcid.org/0000-0003-3348-9538
Yijing He
Southwest Medical University
Jinwei Pang
Southwest Medical University
Ghosh Dipritu
Southwest Medical University https://orcid.org/0000-0001-8236-3785
Long Gu
Southwest Medical University
Yuke Xie
Southwest Medical University
Kecheng Guo
Southwest Medical University
Zheng Bao
Southwest Medical University
Xianhui Zhang
Southwest Medical University
Qianke Tao
Southwest Medical University
Xiancheng Qiu
Southwest Medical University
Qiancheng Mu
Southwest Medical University
Tianqi Tu
Southwest Medical University
Zhaoyang Wang

Southwest Medical University
Yuyan Liao
Southwest Medical University
Yuxuan Zhang
Southwest Medical University
Lihan Zhang
Southwest Medical University
Jiaqi Zhang
Southwest Medical University
Xiao Rao
Southwest Medical University
Chaojie Li
Southwest Medical University
Peng Lu
Southwest Medical University
Chenghao Kuang
Southwest Medical University
Jian Zhou
Southwest Medical University
Xi Kong
Southwest Medical University
Jinyue Zhang
Southwest Medical University
An Huang
Southwest Medical University
Yuanyuan Wu
Southwest Medical University
Lifang Zhang
Southwest Medical University

Article

Keywords: acute brain injury (ABI), multi-omics datasets, Transcriptomics, proteomics

Posted Date: May 12th, 2021

DOI: https://doi.org/10.21203/rs.3.rs-441547/v1

An integrated multi-omics study to identify dynamic molecular alterations associated with acute brain injury

Jianhua Peng[1,2,3#*], Yijing He[2,3,5#], Jinwei Pang[1,2,3#], Ghosh Dipritu[2,3,5#], Long Gu[2#], Yuke Xie[2], Kecheng Guo[2], Zheng Bao[2], Xianhui Zhang[4], Qianke Tao[1], Xiancheng Qiu[1], Qiancheng Mu[1], Tianqi Tu[1], Zhaoyang Wang[1], Yuyan Liao[1], Yuxuan Zhang[1], Lihan Zhang[1], Jiaqi Zhang[1], Xiao Rao[1], Chaojie Li[1], Peng Lu[1], Chenghao Kuang[2], Jian Zhou[1], Xi Kong[4], Jinyue Zhang[4], An Huang[4], Yuanyuan Wu[4], Lifang Zhang[4], Shigang Yin[2,3,5*] and Yong Jiang[1,2,3,4*]

[1] Department of Neurosurgery, The Affiliated Hospital of Southwest Medical University, Luzhou 646000, China.

[2] Laboratory of Neurological Diseases and Brain Function, The Affiliated Hospital of Southwest Medical University, Luzhou 646000, China.

[3] Institute of Epigenetics and Brain Science, Southwest Medical University, Luzhou 646000, China.

[4] Sichuan Clinical Research Center for Neurosurgery, the Affiliated Hospital of Southwest Medical University, Luzhou 646000, China.

[5] Academician (Expert) Workstation of Sichuan Province, the Affiliated Hospital of Southwest Medical University, Luzhou 646000, China.

[#] These authors contributed equally

* Correspondence should be addressed to Dr. Jianghua Peng (pengjianhua@swmu.edu.cn), Dr. Yong Jiang (jiangyong@swmu.edu.cn) & Dr. Shigang Yin (sgyin@swmu.edu.cn)

Abstract

Neuroimmune cells are rapidly transition from a quiescent into an activated state in response to acute brain injury (ABI) threats, but the dynamic molecular alterations are partially understood. Until recently, brain scientists were ineffectual to explore the molecular alterations in human, owing to the obstacles for ABI related brain sample acquisition. Here, we integrated the dynamics of multi-omics datasets in four ABI mice models. Transcriptomics revealed diversification of thermogenesis, synaptic, and neuroinflammatory genes for ABI at the early phase (12H). Transcriptomics and proteomics combined analysis singled out 15 co-variation risk genes for ABIs. Besides, lipid metabolite alteration reflected a discrepancy between permanent ischemic brain injuries and transient ischemic brain injuries at the middle phase (24H). Together, our data elucidate a potential therapeutic resource for ABIs.

Introduction

Acute brain injury (ABI) is one of the leading causes of death and poor prognosis due to limited neurological recovery. Approximately 43%-60% of those hospitalized for traumatic brain injury (TBI)[1-3], 7%-20% of subarachnoid hemorrhage (SAH)[4], and 50%-60% of acute ischemic stroke (AIS) patients[5] suffer long-term disability and even permanently disabled state. The inadequacy of preclinical research on ABI might contribute to the potential for placing patients at unnecessary risk[6]. While traumatic and vascular brain injury are generally considered separately, victims of both TBI and hemorrhagic transformation of AIS often suffer from chemical or mechanical damage to the blood components[7,8]. Alternatively, cerebral infarction remains one of the most severe secondary insults in patients surviving the initial TBI and SAH[9,10].

Despite the increasing advances in surgical treatments, mortality and disability rate from ABI, especially from SAH and TBI, remains still high among brain injury related deaths. Currently, early arterial recanalization following AIS has been shown to improve cerebral blood perfusion and functional outcome[11]. Although thrombolysis is widely recognized to be effective for AIS patients with large vessel occlusions, a large number of stroke subjects are ineligible for recanalization therapies due to unknown symptom onset or other associated limitations in current stroke protocols[12,13]. Previous studies have reported that selective delayed recanalization up to 24 hours after symptom onset resulted in favorable outcomes[14,15], yet the molecular mechanisms are incompletely understood. Mouse middle cerebral artery occlusion (MCAo) models have been used extensively to investigate the mechanisms underlying ischemic stroke, to test the efficacy of candidate drugs, and to predict patient responses. The transient MCAo (TM) and permanent MCAo (PM) are widely used for evaluating the evolution of secondary brain injury in mice with reperfusion and ischemic time-specified differences[16]. Identification of a common cascade of events could have a more significant impact on clinical management approaches of time-dependent cerebral ischemic injuries.

It is common for patients who have had a mild brain injury, ischemia, or microbleeds not to seek immediate medical attention. Disruption of central nervous system (CNS) vasculature and critical barrier structures following ABIs results in the leakage of debris, reactive oxygen species (ROS), and inflammatory mediators into the periphery from the early hours after injuries and lasts until 72 hours post-injury[17,18]. Therefore, understanding the dynamics of these biomarkers is essential for the detection of secondary brain injury in those who may only seek medical care several hours or days after onset. On the other hand, biomarkers that predict responses to the natural course of brain injury could be beneficial for the increase in the odds of survival, of regaining independence, and of becoming asymptomatic[19]. Of the known clinical and physiological events contributing to

secondary ischemic brain damage, homeostasis disorders (e.g., metabolism and thermoregulation disorders) are potential risk factors for ABI outcomes[20,21]. Despite the increasing advances in the knowledge of specific characteristics of those molecules, the complex interaction of these pathomechanisms may make it difficult for targeted pharmacological agents to protect the brain and improve behavioral outcomes[22]. According to these research results, it became apparent that we need integrated analysis of multiple omics data covering more ABI subtypes to discover the molecular cues for the progress of secondary brain injury.

Recently, transcriptomic or proteomic analysis revealed that inflammatory response in ABIs[23-25], enriching the conversion of genetic/molecular discoveries to a certain extent and might provide the novel therapies with reference as well. However, these findings were based on the single or non-predetermined time point of a specific injury (e.g., TBI and AIS). Cerebral gene transcription and protein dynamics in the secondary brain injury process, and whether there are molecular-level commonalities between hemorrhagic and ischemic brain injury have largely remained elusive till recently. On the other hand, metabolomic processes the response to brain injuries can be used for monitoring treatment response, prediction of outcome, in the assessment of or prognosis of post-injury recovery[26]. Since the molecules are dynamically balanced in an individual, a single omics approach could hardly reflect the overall pathophysiological changes objectively and the interrelationships among molecules after brain injuries. Thus, a multi-omics, multiple time phases assay should contribute to a better understanding of the dynamic molecular mechanisms involved in the secondary brain injury process and facilitates the development of therapeutics.

In this study, we utilized four ABI mice models (SAH, TBI, PM, and TM), together with multiple omics assays (transcriptomics, proteomics, metabolomics, and lipidomics), to perform an integrated analysis for ABI subtypes at three progression phases (12H, 24H, and 72H after injury). By integrating multi-omics analysis, we identified and characterized alterations of transcription, translation, and metabolism in the enriched pathways of neuron function and neuroinflammation for the ABI subtypes, among of which, although the PM and TM have shown certain dynamic changes of the transcription level at the late phase of the ABI process, they hold great differences of the protein level and metabolic level at 24H. The lipidomic regulation shift might be a potential factor for the different prognostic effects of PM and TM. Moreover, genes associating with adaptive thermogenesis were upregulated. Finally, we analyzed the clinical data in permanent ischemic stroke and transient ischemic stroke patients concerning acquiring the correlation between body temperature and NIHSS (National Institutes of Health Stroke Scale) score and identified a positive correlation with statistically significant.

Results

Overview of this study

We established four ABI mice models, including SAH, TBI, PM, and TM. Each ABI subtype mice models (17 male wild-type C57BL/6 mice) was composed of three different stages (12H, 24H, and 72H) after brain injuries. All ABI mice models were evaluated by magnetic resonance imaging (MRI)-T2 weighted image (T2WI) (Extended Data Fig.1B) and neurological deficit tests (Extended Data Fig.1C), and all were consistent with previous studies[10,27].

Each ABI mouse model as well as control group (without any treatments) underwent transcriptome, proteome, metabolome, and lipidome assays (Extended Data Fig.1A). Through transcriptome datasets, we identified 626, 1657, 5832 and 5778 DEGs (Differential Expressed Genes) (abs($\log_2$FC) > 1; $P < 0.05$) for ABI mice models compared with control group (Extended Data Fig.1D-E). Hybrid mass spectrometry libraries of proteome, metabolome, and lipidome were

generated as described in method. The detected proteins, metabolites, and lipids were summarized in Supplementary Table 1. All biological replicates for different omics assays in this study have a nice reproducibility (Extended Data Fig.2A,C).

Transcriptome Profile of ABI mice models

Previous studies have reported the dysregulation of gene transcription in ABI mice models[28-30]. However, transcriptome characterization of ABI-derived brain tissue has been limited. To systematically illustrate the transcription dynamics underlying ABIs, which were mainly caused by the secondary injury progresses, we analyzed transcriptome data we generated from ABI mice models at three stages (12H, 24H, and 72H) and identified the DEGs (Extended Data Fig.2B). The normalized counts (see method) of DEGs could reflect the dynamics of gene transcription along with the progression of ABIs.

By comparing gene transcription between ABI subtypes and control group at each stage, we successfully identified 132 (Control vs SAH of 72H) to 3969 (Control vs TM of 72H) DEGs (Extended Data Fig.1D), while all of them had significant up-regulation ($\log_2FC > 1$; $P < 0.05$) (Extended Data Fig.1E). Together, for the number of DEGs, PM and TM were the most in any stage, and SAH was the least (Extended Data Fig.1D-E). This result revealed that ischemic brain injury (PM and TM) at each stage of the ABI process caused more gene transcription alterations than hemorrhagic brain injury (SAH and TBI). In turn, hemorrhagic brain injury (SAH and TBI) or ischemic brain injury (PM and TM) have similar gene transcription patterns respectively. If cross-compared, SAH and ischemic brain injury (PM and TM) both have a large difference in transcription level, but TBI and TM have very similar transcription patterns at the stages (12H and 24H), while TBI' transcription pattern was closer to PM at a late stage (72H) (Extended Data Fig.2B).

Transcription patterns of all DEGs (combined DEGs for each ABI subtype and disease stages; N=5632; Supplementary Table 2) were characterized into 6 clusters through the K-means algorithm (see method) (Fig.1A). The consensus clustering results illustrated that the ABI subtypes and secondary brain injury stages could be distinguished (Fig.1A). SAH and TBI shared the highest transcription level at 12H compared with other ischemic brain injuries, which was also in line with the feature that this group of genes was mainly enriched in the regulation of the blood circulation pathway (cluster 1).

Note that the genes in cluster 2 were mostly characterized by synaptic and neuron functions, and decreased transcription level in all ABI mice models, especially in PM and TM at 72H. This indicated that after the occurrence of ABIs, the transcription of genes related to synapse and neuron function was decreased, which may be related to neuronal dysfunction. Among them, PM and TM may have the most serious neuronal dysfunction at this time point. Interestingly, in cluster 4 and cluster 5, PM and TM have higher transcription levels and more DEGs (47.71% of all DEGs) than other injuries at 72H. These genes were mainly enriched in pathways related to neuroinflammation, such as cytokine, angiogenesis, cell adhesion, IL-6 production, innate immune response, ERK1/2 cascade, and reactive oxygen species metabolic pathway ($P<0.05$, Fisher's Exact Test). This suggested that ischemic ABIs have a more serious neuroinflammatory response at the late stage of the ABIs, which may be related to more severe damage to synapses and neurons in the brain tissues (see cluster 2). It is worth noting that cluster4,5-related DEGs were also enriched in the "regulation of vasculature development" pathway, suggesting that the progress of the ischemic ABIs have a higher transcription of genes that regulate vascular development at the late stage, indicating the angiogenesis and tissue repair activates which was also consistent with previous findings[31].

Although most of DEGs of PM and TM shared similar transcription patterns in the late stage, there were DEGs with opposed transcription patterns (cluster3 and cluster6), which were mainly movement-related (such as cilium movement and microtubule bundle formation/movement, etc.) and temperature adaptation and fat cell growth-related (such as regulation of fat cell differentiation, adaptive thermogenesis, and cold-induced thermogenesis, etc.) genes (Fig.1A). Given that, genes of the two clusters have the potential to be the markers to distinguish PM and TM, because of the transcriptional differences only in PM and TM at 12H, but not in other ABIs.

We also investigated the transcription of 390 genes (cluster 6 in Fig.1A) in PM and TM, which were further classified into two categories (Fig.1B). Based on this finding, these genes have shown a significantly different transcription pattern in PM and TM at 12H (class 1: P=3.15e-07; class 2: P=0.01; Fig.1D). Compared with the control group, DEGs, which are mainly related to temperature regulation, were only highly transcribed in TM and PM at 12H respectively (Fig.1C). To match the findings in ABI mice models with the characteristics of clinical cases, we further performed a correlation analysis between NIH Stroke Scale/Score (NIHSS) and highest body temperature and of ischemic stroke patients during the first 72H after admission. There was a linear growth of body temperature with increasing NIHSS scores in both permanent acute ischemic stroke (PAIS) and transient acute ischemic stroke (TAIS) patients (TAIS: $R = 0.554$, $P < 0.001$; PAIS: $R = 0.304$, $P < 0.001$, Fig.1E). This finding revealed that thrombolysis or endovascular thrombectomy for ischemic stroke has differences in neurological outcomes, and according to previous literature, because of the higher body temperatures during both the intra-ischemic and post-ischemic phases were associated with poorer clinical outcomes[32], so that our results further provide potential molecular evidence for thrombolytic therapy/mechanical thrombectomy combined with mild hypothermia therapy/maintenance of body temperature for ischemic stroke.

The proteomic analysis reveals an increased level of neurological related proteins at 24H

In the previous study of proteomics in ABI mice models, only the disease subtypes or progression stages were considered[19,33]. In our dataset, the Partial Least Squares Discrimination Analysis (PLS-DA) of protein abundance of all ABI mice models illustrated the formation of distinct clusters of the ABI subtypes and the excellent data repeatability of replicates (Extended Data Fig.2D; Supplementary Table 3; see method). All ABI subtypes were distinguished well from each other and shared dynamic protein abundance across each disease progression stage (Extended Data Fig.2C-D).

The comparison between the control group and ABI stages could lead to identifying the differential expressed proteins (DEPs) at each disease progression stage. The DEPs were determined by the $\log_2$ ratio of each protein abundance level to the abundance of the control sample. We applied t-test analysis on all candidates to screen for DEPs with statistical significance. We finally identified, in total, 1201, 1520, and 1514 DEPs at 12H, 24H, and 72H of ABIs respectively (Supplementary Table 1), and heatmaps were used to display them graphically to show the difference in protein abundance between ABI subtypes at the same stage of disease progression (Extended Data Fig.2 C).

The DEPs between ABI subtypes could be potentially useful for distinguishing the subtypes of ABIs. We performed K-Means Cluster analysis (see method) based on the protein abundance of ABI subtypes in the same secondary brain injury progression stage and finally obtained 4, 2, and 3 categories at 12H, 24H, and 72H respectively (Fig.2A, Extended Data Fig.4A-B) and GO enrichment analysis was performed for each category (Fig.2B, Extended Data Fig.4C-D).

As shown in Fig.2A, we could distinguish TM and TBI from SAH and PM by protein abundance at 24H and found that these proteins mainly related to synapse structure and other related protein location (category 2), while in SAH and PM, the proteins related to hydrolase activity and exocytosis were highly translated (category 1) (Fig.2B). This result was significantly different from the other two stages (12H and 72H) and was also different from the previous transcriptome results in the decline of gene transcription levels related to synapse function in TM and PM at 72H (Extended Data Fig.4D), indicating that these genes related to synapse function might share the other regulatory mechanism.

Given symptoms appear suddenly or worsen over time following an ABI, especially within the first 24H after the injury[34], we focused on the biological process pathways of subtype-specific DEPs at 24H for further analysis. The functions of neurons and synapses were closely related to the prognosis of ABIs. Based on the result that the synapse-related functional pathways in category 2 of Fig.2B were highly enriched, we further extracted synapse-related proteins, and analyzed the correlation between their transcription levels and protein abundance (see method), we found that transcription and protein level of all ABI subtypes have a very obvious positive correlation on disease progression at 24H (Fig.2C,). This result was also applicable to the enriched exocytosis-related functional pathways in category 1 of Extended Data Fig.3A.

To further investigate the key molecules related to synaptic function in each ABI subtype, we analyzed the dynamic profile of synapse-related proteins (Fig.2D) and exocytosis-related proteins (Extended Data Fig.3B) of all synapse-related molecules in each ABI subtype (compared with the control group). The Ephb3, mediating developmental processes in the nervous system, was down-regulated in all ABI subtypes at 72H, indicating that it was a key molecule that controls synaptic function in the late stage of ABIs, and its down-regulation may be closely related to impaired synaptic function. Besides, Nrp1 was also down-regulated almost at 72H of ABIs (except TM), indicating that it might also be related to the damage of synaptic function. Interestingly, the Dgkb, which regulates neuron-specific morphological changes including neurite branching and neurite spine formation, was mainly up-regulated in ABI subtypes at 72H (except PM), which could be related to the repairment of synaptic function. It was worth noting that only Lrrtm2 was highly expressed at 24H of TBI, which could be used as a marker gene of TBI. For SAH and TM, Slc8a3 was specifically up-regulated at 12H in SAH and down-regulated at 72H in TM, so it could be used as a marker gene to distinguish these two ABI subtypes. Similarly, Adnp has significantly different protein levels in hemorrhagic ABI (SAH and TBI) and ischemic ABI (PM and TM), indicating that it could be used as a marker for these two types of ABI subtypes.

Transcriptomic and proteomic analysis identified risk factors for ABI mice models

Transcription and translation events should be dynamic during the progression of secondary damage to ABIs. We considered the correlation analysis gene clusters and protein categories and reveal key risk factors that played a major role in ABIs and subtype-specific molecules (Fig.3A).

Based on the gene clusters in Fig.1A, we found that in cluster1 and cluster2, there was no obvious correlation aggregation in SAH; However, in TBI, it has a significant negative correlation aggregation (median: -0.36). Also, PM and TM hold a similar positive correlation aggregation (median: 0.23 and 0.26). This indicates that the disorder of transcription level and translation abundance in the genes of cluster 1 reflected their dynamic function of blood circulation regulation. We further found that TBI also has negative correlation aggregation in cilium movement, microtubule bundle formation, and microtubule-based movement (cluster3). More interesting, except the cluster6, the correlations of PM and TM were almost aggregated to the positive side.

PM has a positive correlation aggregation in cluster1, 2, 3, and 4, especially in cluster3 and cluster4, but there was no obvious correlation aggregation in cluster5.

To further identify the key regulatory molecules in the progression of ABIs, we analyzed the 6 clusters. Taken the intersection for top 10 candidates of 5 screening algorithms by cytohubba plugin in Cytoscape (Closeness, EPC, Degree, Radiality, and MNC), we got 5, 8, 3, 1, 7, and 6 hub genes in cluster1 to cluster6 respectively (Extended Data Fig.5A). The summary of these 30 hub genes was listed in Supplementary Table 4. To further explore the interaction of robust hub genes, we constructed the PPI network by STRING database (Fig.3B). The hub genes in cluster 1 were mainly enriched in behavior and cytosolic calcium ion concentration pathways. The Oxt, encodes a precursor protein that is processed to produce oxytocin and neurophysin I, involved in cognition, adaptation, and regulation of water excretion and cardiovascular functions. The increase in transcription level expression of Oxt could positively regulate the translation level of protein in SAH and PM (Extended Data Fig.5B), but there might be post-translational in TM. The transcription and translation level of Oxt at three stages of four ABI models had significant characteristics, so this gene may be used as a marker gene in different progression stages of ABIs. In cluster 2, these hub genes were highly related to synaptic transmission and regulation of neuronal synaptic plasticity, which was also consistent with the results in Fig.1A, indicating that these 15 hub genes might play an important role in the regulation of synapses and neuronal functions. In SAH and TBI models, transcription level and protein level of Syp had a low correlation ($r = 0.17$; $r = -0.21$) at three stages (Fig.3C), it revealed that there was no obvious regulatory relationship between transcription level and protein level in traumatic/hemorrhagic brain injury subtypes. However, in PM and TM, Syp had a strong positive correlation ($r = 0.99$; $r = 0.99$) between transcriptome and proteome. Hub genes in cluster3 were particularly enriched in the Wnt signaling pathway. Wnt plays an important function in maintaining homeostasis and is involved in the formation of the brain and multi-synaptic globular rings[35,36]. MKI67, the hub gene of cluster 4, encodes a nuclear protein associated with cellular proliferation. In cluster 5 and cluster 6, hub genes were mainly enriched in pathways related to abiotic stimulus, cytokine, apoptotic and inflammatory response.

Overall, the identification of risk factors (hub genes), and particularly of ABI subtype-specific molecules underscores their potential roles in ABI progression.

Metabolic Characteristics of ABI

These dynamic transcriptomic and proteomic changes in ABIs promoted us to study alterations in the metabolic process. For ABIs, probably together with astrocytic and microglial activation and induction of a metabolic disorder state that can induce secondary injury events, offering several potential clinical biomarkers and therapeutic targets[37]. We explored whether the alterations in transcription and translation levels could modulate the metabolites. Because changes of genes in transcription or translation levels can lead to broad metabolites alterations due to modulation of metabolic pathways.

To manipulate the dynamic changes in metabolites at different stages of ABIs, we utilized LC-MS to perform metabolomic and lipidomic assays (Extended Data Fig.1A, Supplementary Table 5). Further abundance profile indicated high repeatability of lipidomic and metabolomic datasets (Extended Data Fig.2C). Given our focus on the metabolites alterations, we characterized the detected metabolites into four categories according to the public metabolic molecules database (Fig.4A, Extended Data Fig.6B-C; see method): lipids, nucleotides, organic compounds, and others. The organic compounds accounted for the vast majority in the three stages (early stage:

52.63%; mid-stage: 52.67%; and late-stage: 52.63%) in the four ABIs. Among them, we found that lipids (9%) hold dynamic changes. The nucleotides category (9.33%) was significantly higher in TM compared to the other ABI subtypes at 24H. Generally, the metabolome profile exhibited more altered patterns between PM and TM at 24H (Fig.4A). Besides, this finding was also consistent with the results in 12H and 72H (Extended Data Fig.6B); and could catch out attention to the difference in metabolites caused by the progression stages of ABIs.

Inspection of differential expressed metabolites (DEMs) (Fig.4A, Extended Data Fig.6A, and Supplementary Table 1) and KEGG enrichment at each progression stage of ABIs revealed the changes in metabolic pathways. We classified each pathway of DEMs and found that metabolism accounted for 42.93%, 49.96%, 44.2% at 12H, 24H, and 72H (average at four ABI models), Organismal Systems accounted for 29.48%, 26.92%, and 28.49%, and human disease accounted for 14.27%, 10.76%, 15.15% (Fig.4B). The top 10 KEGG pathways of Metabolism and Human Disease in the four ABI models were displayed in Extended Data Fig.7A-C.

Consequently, further analysis of filtering out low-quality values (see methods) suggested that only 1380(12H), 1266 (24H), and 1380 (72H) lipid features could be used for downstream analysis. Differential expressed lipids (DELs) at each stage of ABIs were identified in a high frequency of phosphatidylethanolamine (PE), phosphatidylcholine (PC), Ceramides (Cer), and lysophosphatidylcholine (LPC) at 24H (Fig.4C). Moreover, in 12H and 72H, PE, PC, and Simple Glc series (CerG1) categories accounted for the major proportion (Extended Data Fig.7D).

As the progression of ABIs, we noticed that DELs for CerG1 gradually decrease in the SAH (12H: 23.53%; 24H: 10.61%; 72H: 6.25%; Extended Data Fig.8). But in TBI, CerG1 accounted for the largest proportion in 72H (27.78%). This suggests a potential molecular marker for distinguishing the SAH and TBI. Moreover, PM and TM occupied more dynamic alterations for CerG1, which both gone through along with the ABI progression according to the patterns of "high- low- high" in PM (12H: 22.52%; 24H: 6.78%; 72H: 32.54%) and TM (12H: 13.64%; 24H: 4.17%; 72H: 31.82%) (Fig.4C, S8). Interestingly, in TM, we found DELs in PE accounted for 27.27% (12H) and 18.18% (72H) proportion at the early and late stages respectively; however, we did not detect PE expression at 24H. This suggests that cephalin-related lipids mainly changed in the early and late stages of TM, but at 24H, it preferred the regulation of lecithin-related lipids changes. Also, we found 12H and 72H had more overlapped DELs (Fig.4D) in four ABI subtypes. This analysis revealed that there might be more metabolites alterations in the mid-stage of ABIs (24H) compared with the early (12H) and late stages (72H).

These metabolic analyses identified the dynamic alterations in metabolites, especially in lipids, associated with the progression of ABIs, supporting the roles for metabolic disorders in ABIs.

Dynamic lipid alterations are associated with PM and TM

Metabolomics analysis revealed that the abundance of a batch of lipid molecules changed dynamically in PM and TM (Fig.4A, Extended Data Fig.6B). These lipid alterations may pinpoint the genes involved in the lipids metabolic process. We considered the analysis of lipid-related genes for PC, PE, Cer, CerG1, and PS (downloaded from Mouse Genome Informatics; see method) (Fig.5A and Supplementary Table 6). The abundance of genes and proteins were correlated well regardless of PM and TM progression in PC-related genes. Compared with TM, the log2FC (versus Ctrl) of PE-related protein Esyt1, CerG1-related proteins Gba and Gba2, and Cer-related protein Agk in PM showed a gradual increase trend during the first 72 hours. For PS-related proteins, the log2FC of Syt12 (versus Ctrl) was higher at 12H, decreased at 24H in PM compared with TM, then back to a high level (log2FC of PM versus log2FC of TM) at 72H (Fig.5B, Supplementary

Table 7). This result was confirmed that in the late stage (72H) of ischemic brain injury (PM and TM), lipid-related proteins involved in an important pathological process of ABI. However, PM and TM always occupied an inconsistent pace in the abundance regardless of the transcription and translation levels and ABIs progressions.

To further explore the lipids alterations in PM and TM, we analyzed in detail the abundance changes of DELs in PM and TM with the progress of ABIs. It was remarkable that we found similar lipids abundance patterns associated with PM and TM in 12H and 72H (Fig.5C). However, just like the dynamic changes at the transcription and protein levels, the abundance of DELs also showed dynamic changes in 24H. Among them, almost all Cer and PS were down-regulated, and only CerG1 was up-regulated in PM. As for PE and PC, which are the largest portion of lipids in brain tissues, DELs abundances of PM and TM hold a very obvious mutually exclusive pattern. Based on the results above, we found that the Cer and PS of PM were greatly decreased compared to TM, and these two types of lipid molecules appear to have a positive role in neurological function post stroke[38,39]. These data provide molecular evidence of ischemic time-depended secondary brain injury related to lipid metabolism.

Discussion

The key to developing effective brain injury treatments is to better understand and determine the exact mechanism of the secondary pathology associated with ABI. Current guidelines are agreed on the general principles of early management or medical care for ABI patients[40,41]. However, the progression and survival prediction of patients with late-stage ABI are extremely challenging obstacles to successful treatment selection, partly due to a lack of understanding of the complex pathophysiological changes during secondary brain injury.

Here, we reported an integrated omics analysis of ABI mice models, which uncovered molecular alterations associated with ABIs. A total of 15 co-variation risk factors were identified as key regulators for secondary pathophysiological changes of ABIs. The relationship between transcriptome and proteome patterns and prognosis may facilitate the precise treatment and evaluation of late-stage ABI patients.

In particular, for the early stages of ABIs, widespread transcriptome abnormalities with prominent signatures of body temperature in the prognosis of ischemic brain injuries. The relationship between abnormal body temperature and ABI severity and clinical outcome has been reported previously[20,42], but the molecular mechanism behind it, especially the regulatory factors of gene and protein network under the multi-omics model, has not been revealed yet. Our results confirmed that thermoregulation-related genes, including 20 genes were differentially expressed under cerebral infarction. Previous studies have reported that the *Wnt10b*, *Dio2*, *Gadd45g,* and *Lcn2* can regulate the thermogenic function of adipose tissue under stress[35,43-45]. Recently, the epigenetic regulator *Kdm6b* is reported as a temperature-sensitive factor[46]. On the other hand, inflammatory cytokine (e.g. interleukin-6) is reported to be associated with elevated body temperature after stroke[47]. In this study, inflammation-related pathways such as interleukin-6 production, cytokine-mediated signaling pathway, and regulation of innate immune response are significantly changed in ABI brains. Our transcriptomics/proteomics combined analysis provides potential molecule targets for the regulation of body temperature after ischemic ABIs.

Specifically, although the primary injury mechanism is considered different, traumatic and hemorrhagic injury share dysregulation of cerebral blood flow, resulting in secondary ischemic injury. For ischemic stroke, if reperfusion is not achieved in the subacute phase, a delayed phase (days to weeks after symptom onset) may occur in which ischemic injury is further exacerbated

by secondary oxidative stress, brain edema, neuroinflammation, and other associated and relevant deleterious molecular mechanisms. Thus, the multi-omics dynamic analysis would provide evidence of the effect of ischemic time on brain injury from a molecular level. Between the two subtypes of ischemic ABI models, PM and TM, these ischemic injuries harbored few differences in their transcriptomic signatures. However, we found that lipidomics of PM and TM revealed variations between them during the first 72H after injury, showing that lipid metabolism is sensitive to ischemia, which is consistent with the previous investigation[48].

Based on the integrated omics dataset of ABI mice models, we have established a resource database of disease progression and molecular pathology characteristics of ABI to allow researchers to understand and evaluate this disease more comprehensively. Through the results of transcriptome and proteomics, we have identified the genes related to temperature disturbance in the early stage of ischemic ABI and the key molecules in the regulatory network of the entire disease progression. In addition to thermoregulation-related pathways, other pathways related to early brain damage such as synaptic plasticity correlations and neurofilament-based process were significantly changed in ABI models, which have been reported as neurobiological foundations for biomarker applications in brain injury and neurodegeneration[49]. These results will bring about substantial assistance for early intervention and diagnosis of ischemic ABIs, and will also provide a molecular basis for the development of ABI therapeutic drugs.

In summary, our integrated omics dataset focused on ABI providing the global characteristics of transcripts, proteins, and metabolites. Based on our observations of divergence changes in multiple omics characteristics for distinct progression of ABIs, we found that correlation analysis combined with transcriptomics and proteomics data can accurately reflect ABIs. Also, the changes in metabolites, especially lipid metabolites, reflect the secondary brain injury progression stage of ABIs. These results strongly suggest that the treatment and rehabilitation of ABI patients should focus on changes in brain metabolites in both traumatic/hemorrhagic and ischemic ABIs for effective, individualized treatment strategies.

Methods

Animals and ABI mice models. All experiments were approved by the Southwest Medical University Animal Studies Committee (201903-105). We followed the Guide for the Care and Use of Laboratory Animals of China. Male C57BL/6 wild-type mice were purchased at 10-12 weeks of age, housed in a pathogen-free facility with access to food and water. Our methods also included randomization, blinding, and statistical criteria consistent with ARRIVE guidelines (Animals in Research: Reporting In vivo Experiments). All surgical procedures were conducted under aseptic conditions. For RNA sequencing, (N = 9) each group at each time point (dissolved with TRIzol and then the lysates of three mice in each group were pooled into one sample). For LC-MS/MS, (N = 8) each group at each time point.

The SAH mouse model was performed by endovascular perforation as previously described with slight modifications[29]. Briefly, anesthesia was induced by inhalation of 3% isoflurane in a nitrous oxide/oxygen mixture (70% oxide, 30% oxygen) and maintained by 1.5% isoflurane administered through a facemask. After the right internal carotid artery (ICA) was exposed, a 5-0 prolene filament was introduced into the right external carotid artery (ECA) and advanced through the ICA until the resistance was felt, further advanced 3 mm to induce arterial rupture. Subsequently, the filament was immediately withdrawn. Body temperature was maintained at 37 ± 0.5 °C throughout the procedure using a heating pad.

The TBI mouse model was induced under isoflurane anesthesia using a controlled cortical impact (CCI) technique[27]. Briefly, the animals were anesthetized with 1.5% isoflurane and checked for pain reflexes. A 3 mm right lateral craniotomy centered at 2.7 mm lateral from the midline and 3 mm anterior to lambda was performed with a motorized drill. The skull was removed without disrupting the dura. The CCI was produced with a pneumatic cylinder (Precision Systems and Instrumentation) using a 3 mm diameter flat-tip impounder (velocity, 3 m/s; dwell time, 100 ms; depth, 1.0 mm). A polyvinylidene fluoride skull cap was secured over the craniotomy and sealed. Body temperature was maintained at 37 ± 0.5 °C throughout the procedure using a heating pad. The anesthetized mice were wrapped in a blanket (37 °C) until recovered and were able to freely ambulate.

For the ischemic stroke mice models, the transient focal cerebral ischemia was produced by the right cerebral artery occlusion (MCAO) with slight modifications[50]. Briefly, under isoflurane anesthesia (3% induction, 1.5% maintenance), mice were placed in a supine position, a midline incision was made on the neck, and the right common carotid artery (CCA) was exposed. A 6-0 nylon monofilament was inserted through the stump of ECA into the ICA and advanced into the middle cerebral artery until light resistance was felt (12 mm). After 90 min of MCAO, reperfusion was initiated by withdrawing the nylon monofilament. Body temperature was maintained at 37 ± 0.5 °C throughout the procedure using a heating pad. The same procedure is performed with the permanent MCAO model, but no reperfusion until euthanasia.

Patients. A total of 41 transient ischemic stroke patients (who have received thrombolysis or thrombectomy therapy at the time of data collection) and 119 permanent ischemic stroke patients (who have not received any thrombolysis or thrombectomy therapy at the time of data collection) were included for body temperature analysis. The collection of patient data was approved by the ethics committee of the Affiliated Hospital of Southwest Medical University (No. KY2020161).

Magnetic resonance imaging (MRI) scan. MRI was performed on a 7.0 Tesla animal scanner (Bruker Biospin, Germany) as previously described[27]. Mice were anesthetized by isoflurane (induction, 3% isoflurane with 1 L/min O2; maintenance, 1.5% isoflurane with 1 L/min O2), and mounted in a Bruker animal bed. T2-weighted images were acquired using RARE (repetition time = 4000, echotime = 45, RARE factor 8, 0.5 mm, field of view 2.5 cm, 256 × 256). Analysis and image reconstruction was performed with Bruker ParaVision 6.0 software (Bruker Biospin, Germany).

RNA library preparation and sequencing. RNA per sample was extracted using TRIzol RNA Isolation Reagents (Invitrogen, USA) according to the manufacturer's instructions. After RNA purity was checked using the NanoPhotometer® spectrophotometer (IMPLEN, CA, USA), their degradation and contamination were monitored on 1% agarose gels. RNA concentration and integrity were measured using Qubit® RNA Assay Kit in Qubit®2.0 Flurometer (Life Technologies, CA, USA) and the RNA Nano 6000 Assay Kit of the Bioanalyzer 2100 system (Agilent Technologies, CA, USA), respectively.

A total amount of 3 μg RNA per sample was used as input material for the RNA sample preparations. Sequencing libraries were generated using NEBNext® UltraTM RNA Library Prep Kit for Illumina® (NEB, USA) following the manufacturer's recommendations and index codes were added to attribute sequences to each sample. Briefly, mRNA was purified from total RNA using poly-T oligo-attached magnetic beads. Fragmentation was carried out using divalent cations

under elevated temperature in NEBNext First Strand Synthesis Reaction Buffer (5X). First strand cDNA was synthesized using a random hexamer primer and M-MuLV Reverse Transcriptase (RNase H-). Second strand cDNA synthesis was subsequently performed using DNA Polymerase I and RNase H. Remaining overhangs were converted into blunt ends via exonuclease/polymerase activities. After adenylation of 3' ends of DNA fragments, NEBNext Adaptor with hairpin loop structure was ligated to prepare for hybridization. To select cDNA fragments of preferentially 250~300 bp in length, the library fragments were purified with the AMPure XP system (Beckman Coulter, Beverly, USA). Then 3 μl USER Enzyme (NEB, USA) was used with size-selected, adaptor-ligated cDNA at 37°C for 15 min followed by 5 min at 95 °C before PCR. Then PCR was performed with Phusion High-Fidelity DNA polymerase, Universal PCR primers, and Index (X) Primer. At last, PCR products were purified (AMPure XP system) and library quality was assessed on the Agilent Bioanalyzer 2100 system. The clustering of the index-coded samples was performed on a cBot Cluster Generation System using TruSeq PE Cluster Kit v3-cBot-HS (Illumia) according to the manufacturer's instructions. After cluster generation, the library preparations were sequenced on an Illumina platform and 150 bp paired-end reads were generated.

Protein library preparation and sequencing. All samples, including mixed pool samples, were digested with Trypsin per APT's internal SOP for FASP digestion. Add DTT to a final concentration of 10mM, boiling water bath for 15min, cooling to room temperature, adding 200μL UA buffer (8M Urea, 150mM Tris-HCl, pH8.0) to mix well, transferring to 10KDa ultrafiltration tube, centrifuged at 14000g for 30min. Add 200μl UA buffer and centrifuge at 14000g for 30min, discard the filtrate. Add 100μL IAA (50mM IAA in UA), shake at 600rpm for 1min, protect from light and room temperature for 30min, and centrifuge at 14000g for 20min. Add 100μL UA buffer, centrifuge at 14000g for 20min, and repeat 3 times. Add 100μL NH4HCO3 buffer (50mM), centrifuge at 14000g for 20min, and repeat twice. Add 40μL NH4HCO3 buffer (2μg Lys-C), shake at 600rpm for 1min at 37°C for 4h, then add 2μg Trypsin to the sample at 37°C for 16h. Replace with a new collection tube and centrifuge at 14000g for 15min. Add 40μL of NH4HCO3 buffer (50mM) and centrifuge at 14000g for 30min, and collect the filtrate. OD280 measures the peptide concentration. Take 100μg Pool mixed peptides, use the HPRP method for fractionation, and collect all the components. After the peptides of each component were lyophilized, they were reconstituted with 10μl 0.1% FA, and the peptide concentration was determined by OD280. Then take out 2μg peptide fragments, mix with an appropriate amount of iRT standard peptide fragments, and conduct DDA mass spectrometry detection. The mass spectrometry analysis time of each component is 2h.

All fractions for Data Dependent Acquisition (DDA) library generation were injected on a Thermo Scientific Q Exactive HF mass spectrometer connected to an Easy nLC 1200 chromatography system (Thermo Scientific). 2μg peptides were first loaded onto an EASY-SprayTM C18 Trap column (Thermo Scientific, P/N 164946, 3um, 75um*2cm), then separated on an EASYSprayTM C18 LC Analytical Column (Thermo Scientific, ES803, 2um, 75um*50cm) with a linear gradient of buffer B (80% acetonitrile and 0.1% Formic acid) at a flow rate of 250 nl/min over 120 min. MS detection method was positive ion, the scan range was 300-1650 m/z, resolution for MS1 scan was 60000 at 200 m/z, target of AGC (Automatic gain control) was 3e6, maximum IT was 25ms, dynamic exclusion was 30.0s. Each full MS–SIM scan followed 20 ddMS2 scans. Resolution for MS2 scan was 15000, AGC target was 5e4, maximum IT was 25ms and the normalized collision energy was 27eV.

Each sample peptide was analyzed by LC-MS/MS operating in the data-independent acquisition (DIA) mode by Shanghai Applied Protein Technology Co., Ltd. Each DIA cycle contained one full MS–SIM scan, and 30 DIA scans covered a mass range of 350–1650 m/z with the following settings: SIM full scan resolution was 60,000 at 200 m/z; AGC 3e6; maximum IT 50ms; profile mode; DIA scans were set at a resolution of 30,000; AGC target 3e6; Max IT auto; normalized collision energy was 30eV. Runtime was 120min with a linear gradient of buffer B (80% acetonitrile and 0.1% Formic acid) at a flow rate of 250 nl/min. QC samples (pooled sample from an equal aliquot of each sample in the experiment) were injected with DIA mode at the beginning of the MS study and after every 6-8 injections throughout the experiment, which was used to monitor the MS performance.

Metabolism library preparation and sequencing. Take out the sample at -80°C, weigh 60mg sample, add 200ul water MP homogenate, vortex for the 60s, add 800ul methanol acetonitrile solution (1:1, v/v), vortex for 60s, low-temperature ultrasound for 30min, 2 times, Precipitate the protein at -20°C for 1 hour, centrifuge at 14000 rcf for 20 min at 4°C, take the supernatant and freeze-dry, and store the sample at -80°C. The samples were separated by Agilent 1290 Infinity LC Ultra-High-Performance Liquid Chromatography (UHPLC) HILIC column; column temperature was 25°C; flow rate was 0.3 mL/min; mobile phase composition A: water + 25 mM ammonium acetate + 25 mM ammonia, B: Acetonitrile; the gradient elution procedure is as follows: 0-0.5 min, 95% B; 0.5-7 min, B linearly changes from 95% to 65%; 7-8 min, B linearly changes from 65% to 40%; 8-9 min, B maintained at 40%; 9-9.1 min, B changed linearly from 40% to 95%; 9.1-12 min, B maintained at 95%; throughout the analysis process The sample is placed in the 4°C autosamplers. To avoid the influence caused by the fluctuation of the detection signal of the instrument, a random order is adopted for continuous analysis of samples. QC samples are inserted into the sample queue to monitor and evaluate the stability of the system and the reliability of experimental data. Electrospray ionization (ESI) positive ion and negative ion modes were used for detection. The samples were separated by UHPLC and analyzed by Agilent 6550 mass spectrometer. The ESI source conditions are as follows: Gas Tem: 250°C, Drying gas: 16 L/min, Nebulizer: 20 psig, Sheath gas Tem: 400°C, sheath Gas Flow: 12 L/min, Vcap: 3000 V, Nozzle voltage: 0 V. Fragment: 175 V, Mass Range: 50-1200, Acquisition rate: 4 Hz, cycle time: 250 ms.

After the samples were tested, the AB Triple TOF 6600 mass spectrometer was used to identify the metabolites, and the primary and secondary spectra of the QC samples were collected. The ESI source conditions are as follows: Ion Source Gas1 (Gas1): 40, Ion Source Gas2 (Gas2): 80, Curtain gas (CUR): 30, source temperature: 650°C, IonSapary Voltage Floating (ISVF) ±5000 V (positive and negative) Two modes); the secondary mass spectrum is obtained by information-dependent acquisition (IDA), and the high sensitivity mode is adopted, Declustering potential (DP): ±60 V (both positive and negative modes), Collision Energy: 35 ± 15 eV, IDA setting The following Exclude isotopes within 4 Da, Candidate ions to monitor per cycle: 10. The data collection is segmented according to the mass range, 50-300, 290-600, 590-900, 890-1200, thereby expanding the collection rate of the secondary spectrum, each method collects four repetitions per segment. The collected data were used to identify the structure of metabolites using self-built MetDDA and LipDDA methods. After the sample is tested, use AB Triple TOF 6600 mass spectrometer to collect the primary and secondary spectra of the sample.

The ESI source conditions after HILIC chromatographic separation are as follows: Ion Source Gas1(Gas1): 60, Ion Source Gas2(Gas2): 60, Curtain gas (CUR): 30, source temperature: 600°C, IonSapary Voltage Floating (ISVF)± 5500 V (both positive and negative modes); TOF MS scan

m/z range: 60-1000 Da, product ion scan m/z range: 25-1000 Da, TOF MS scan accumulation time 0.20 s/spectra, product ion scan accumulation time 0.05 s/ spectra; the secondary mass spectrum is obtained by information-dependent acquisition (IDA), and the high sensitivity mode is adopted, Declustering potential (DP): ±60 V (both positive and negative modes), Collision Energy: 35±15 eV, IDA The settings are as follows: Exclude isotopes within 4 Da, Candidate ions to monitor per cycle: 6 (Shanghai Applied Protein Technology, Shanghai, China).

Lipid library preparation and sequencing. Lipid extraction and mass spectrometry-based lipid detection were performed by Applied Protein Technology. And a separate sample in each group and mix them equally together to create a pooled QC sample. QC samples were inserted into the analysis queue to evaluate the system stability and data reliability during the whole experimental process. Precisely weigh 30 mg of the sample and transfer it to a 2 mL centrifuge tube pre-installed with an appropriate number of magnetic beads, add 200 μL of 4°C water, and put it in the solution. Flash freezing in nitrogen for 5 seconds, and homogenize it with MP homogenizer (24×2, 6.0M/S, the 60s, three times). Add 240μL of pre-cooled methanol, vortex to mix, add 800μL of MTBE, vortex to mix, sonicate in a low-temperature water bath for 20 minutes, place at room temperature for 30 minutes, and centrifuge at 14000 g at 10°C 15 min, take the upper organic phase, blow dry with nitrogen, and store the sample at -80°C. The samples were separated using UHPLC Nexera LC-30A ultra-high performance liquid chromatography system. The column temperature is 45°C; the flow rate is 300 μL/min. Mobile phase composition A: 10 mM ammonium formate acetonitrile aqueous solution (acetonitrile: water=6:4, v/v), B: 10 mM ammonium formate acetonitrile isopropanol solution (acetonitrile: isopropanol=1:9, v/v). The gradient elution procedure is as follows: 0-2 min, B is maintained at 30%; 2-25 min, B changes linearly from 30% to 100%; 25-35min, B is maintained at 30%. The sample is placed in the 10°C autosamplers during the entire analysis. IToavoid the influence caused by the fluctuation of the detection signal of the instrument, a random sequence is adopted to carry out continuous analysis of the sample.

Electrospray ionization (ESI) positive ion and negative ion modes were used for detection. Mass spectrometer (Thermo ScientificTM) performs mass spectrometry analysis. The mass-to-charge ratios of lipid molecules and lipid fragments are collected according to the following method: 10 fragment patterns (MS2 scan, HCD) are collected after each full scan. MS1 has a resolution of 70,000 at M/Z 200, and MS2 has a resolution of 17,500 at M/Z 200. Lipid identification (secondary identification), peak extraction, peak alignment, and quantification were assessed with LipidSearch software version 4.1 (Thermo Scientific™). In the extracted ion features, only the variables having more than 50% of the nonzero measurement values in at least one group were kept (Shanghai, China).

Transcriptome analysis. The raw fastq files were trimmed using trim galore (version 1.18) to remove adaptor sequences and low-quality reads. Then FastQC (version 0.11.9) was used for quality control. The remaining reads were aligned to the GRCm38 mouse genome using HISAT2 (v2.2.0) with default parameters and further filtered with samtools (version 1.10, parameters used: samtools view -F 1804 -f 2 -q 30). Gene counts were calculated from the mapped reads using featureCounts (v2.0.1) with the Ensembl gene annotation (version mm10). Subsequently, TPM (Transcripts Per Kilobase of exon model per Million mapped reads) in each gene was calculated for subsequent analysis.

Proteome analysis. The DDA data was searched by Maxquant software (Maxquant_1.5.3.17), and the database was downloaded by human uniprot, and the iRT peptide sequence was added to the database (>Biognosys|iRTKit|Sequence_fusionLGGNEQVTRYILAGVENSKGTFIIDPGGVIRGTFIIDP AAVIRGAGSSEPVTGLDAKTPVISGGPYEYRVEATFGVDESNAKTPVITGAPYEYRDGL DAASYYAPVRADVTPADFSEWSKLFLQFGAQGSP FLK). The search parameters are set as follows: Enzyme is trypsin, max miss cleavage site is 2, fixed modification is Carbamidomethyl (C), dynamic modification is set to Oxidation (M) and Acetyl (Protein N-term), the protein identified by database search must pass The set filter parameter FDR<1%. Import the original raw files and search results into the Spectronaut software to build the Spectral Library. DIA data uses Spectronaut software (Spectronaut Pulsar X_12.0.20491.4) for data processing, and the database is the same as the database used for database construction. The software parameters are set as follows: retention time prediction type is set to dynamic iRT, interference on MS2 level correction is enabled, cross run normalization is enabled, all results must pass the set filter parameter Q Value cutoff is 0.01 (equivalent to FDR<1%).

Metabonome analysis. The raw MS data (wiff.scan files) were converted to MzXML files using ProteoWizard MS Convert version 3.0.6458 before importing into freely available XCMS software. For peak picking, the following parameters were used: centWave m/z = 25 ppm, peak width = c (10, 60), prefilter = c (10, 100). For peak grouping, bw = 5, mzwid = 0.025, minfrac = 0.5 were used. In the extracted ion features, only the variables having more than 50% of the nonzero measurement values in at least one group were kept. Compound identification of metabolites by MS/MS spectra with an in-house database established with available authentic standards. After normalized to total peak intensity, the processed data were uploaded before importing into SIMCA-P (version 14.1, Umetrics, Umea, Sweden), where it was subjected to multivariate data analysis, including Pareto-scaled principal component analysis (PCA) and orthogonal partial least-squares discriminant analysis (OPLS-DA). The 7-fold cross-validation and response permutation testing were used to evaluate the robustness of the model. The variable importance in the projection (VIP) value of each variable in the OPLS-DA model was calculated to indicate its contribution to the classification. Metabolites with the VIP value >1 were further applied to Student's t-test at a univariate level to measure the significance of each metabolite, the p values less than 0.05 were considered as statistically significant.

Lipidome analysis. LipidSearch is used for peak identification, peak extraction, lipid identification (secondary identification), and other processing. The main parameters are precursor tolerance: 5 ppm, product tolerance: 5 ppm, production threshold: 5%. Perform data analysis on the data extracted by LipidSearch, including univariate statistical analysis, multivariate statistical analysis, hierarchical cluster analysis, and correlation analysis. Univariate statistical analysis includes the Student's t-test/non-parametric test and multiple variation analysis. Multivariate statistical analysis includes unsupervised principal component analysis (PCA) analysis, supervised least squares discriminant analysis (PLS-DA), and orthogonal partial least squares discriminant analysis (OPLS-DA).

Differential analysis. Differential expressed genes (DEGs) was evaluated using DESeq2 package in R (version 4.2.0), using p-adjust < 0.05 and |log2FC| > 1 as cutoffs to define the DEGs. Raw protein abundance data was used to identify significantly changed proteins with unpaired two-

sided Student's t-tests (Welch t-test). Proteins with p-value < 0.05 and |log2FC| > 0.585 were considered as significantly changed proteins. For metabolome and lipidome, the effect of VIP (Variable Importance for the Projection) value was fully considered while performing the Student's t-tests. VIP is used to measure the intensity and explanatory power of the expression pattern of each metabolite on the classification and discrimination of each group of samples, thereby assisting the screening of marker metabolites. Only molecules whose p-value < 0.05 and VIP > 1 were considered as significant.

Enrichment analysis of DEGs. K-means clustering was performed to identify transcriptome-typical clusters of acute brain injury models. 5632 differential expressed genes of four models in three-time points compared with control were selected for clustering. We calculated the Within-Cluster-Sum of Squared Errors (WSS) for different values of k and chose the k for which WSS becomes first starts to decrease significantly. To better characterize transcriptome clusters, we sought to identify the biological pathways distinctly associated with each cluster. A subset of these pathways with biological relevance in specific biological functions was selected for display in Fig.1A, the differential expressed genes involved in the pathway are marked with gray lines, and the significantly enriched genes in each cluster are marked with the color as same as the cluster.

Correlation analysis of gene expression and protein abundance. To identify differentially expressed genes with an association between the mRNA expression and protein translation, we calculated the Pearson correlation coefficient (PCC) for each gene across three-time points between the log2foldchang of RNA expression and the corresponding protein translation levels in each model. We also calculated the PCC for each gene across four acute brain injury models in each time point to explore the relationships between the different models. To limit our analysis to mRNA/protein pairs reflecting robust changes, only genes with a translational level in our proteomics were analyzed.

Hubgenes Identification. CytoHubba is a Cytoscape plugin that allows the use of several topological analysis algorithms, including MCC, DMNC, MNC, Degree, EPC, BottleNeck, EcCentricity, Closeness, Radiality, Betweenness, and Stress. These approaches can be used to predict and explore important nodes in PPI networks. In our study, the intersection of the top 10 genes from 5 topological analysis algorithms (MNC, Radiality, Degree, EPC, Closeness) was chosen as hub genes. Only hub genes with a translational level were performed correlation analysis in Fig.2B and Extended Data Fig.5B.

Protein-Protein Interaction Network Construction. We uploaded the hub genes in each cluster to the STRING online database, chose confidence > 0.9 as the screening criteria. The related nodes were also shown in the current network. The visualized PPI network was performed by Cytoscape (version 3.6.1). The node size represents degree and the edge size represents the combined score.

Classification of metabolites and enrichment pathways. Metabolites KEGG pathway annotation was performed through http://cloud.aptbiotech.com/#/main-page, a website dedicated to proteome, PTM modification, metabonomics, and biomedicine structural characterization. After KEGG pathway annotation, KEGG pathways classification and metabolites classification were also completed on this website.

Genes enriched in lipid-associated pathways. To observe the correlation between genes and lipids, we downloaded the pathways related to Several major categories of lipids (phosphatidylethanolamine, phosphatidylcholine, phosphatidylserine, Ceramides, Simple Glc series) from Mouse Genome Informatics (http://www.informatics.jax.org/). The genes involved in these pathways are extracted to draw the expression profile by the Heatmap function in R.

Statistical analysis. Visualization of the statistical analyses was performed using R (version 4.2.0). We applied Partial Least Squares Discriminant Analysis (PLS-DA) from the mixOmics Package in R to distinct different models. Gene ontology enrichment and Kyoto Encyclopedia of Genes and Genomes (KEGG) enrichment were performed using the clusterProfiler Bioconductor package. Venn diagrams were drawn using the VennDiagram package. Heatmap function from the R packages Complex Heatmap was used to cluster and visualization. We used unpaired two-sided Student's t-tests (Welch t-test) for normally distributed data in which two comparison groups were involved. In the case of multiple comparisons, Benjamini and Hochberg correction was then performed for the raw p-value to obtain the q-value. Pearson correlation analysis was performed to determine correlations between neurological score and body temperature variables of ischemic stroke patients. We set the significance level at α=0.05.

Data availability

The transcriptomic data that support the findings of this research are available through the National Center for Biotechnology Information under accession number PRJNA719247.

Acknowledgment

This work was supported by grants from the Young Elite Scientist Sponsorship Program by the China Association for Science and Technology, and the National Natural Science Foundation of China (81771278, 81801176, 81971132); the Sichuan Science and Technology Program (2019JDTD0004).

Author contributions

J.H.P., Y.J., and S.G.Y. conceived the project. J.W.P., Y.K.X., K.C.G., X.H.Z., Q.K.T., X.C.Q., Q.C.M., T.Q.T., and Y.X.Z. created the ABI mice models and performed mass spectrometry experiments. Y.Y.L., C.J.L., P.L., C.H.K., and X.K. performed the RNA extraction and RNA-seq libraries construction. Y.J.H. performed the transcriptomic, proteomic, metabolic, and lipidomic data processing and supervised most of the analyses. L.G., L.H.Z., and G.D. performed the integrated omics data analysis and transcripts and protein functional enrichment analysis. Y.J.H. performed the statistical analysis work. J.H.P., J.W.P., J.Q.Z., X.R., Z.Y.W., and J.Z. performed the MRI assays and clinical data statistics and analysis work. L.F.Z., Y.J., and S.G.Y. contributed to the methodology and resources. J.H.P., Y.J.H., G.D,. Y.J., and S.G.Y. wrote the manuscript. All authors reviewed the manuscript and discussed this study.

Conflict of interest

The authors declare no competing financial interests.

Additional information

Correspondence and requests for materials should be addressed to Y.J., S.G.Y., or J.H.P.

Reference

1. Jiang, J.Y. *et al.* Traumatic brain injury in China. *Lancet Neurol* **18**, 286-295 (2019).
2. Ma, V.Y., Chan, L. & Carruthers, K.J. Incidence, prevalence, costs, and impact on disability of common conditions requiring rehabilitation in the United States: stroke, spinal cord injury, traumatic brain injury, multiple sclerosis, osteoarthritis, rheumatoid arthritis, limb loss, and back pain. *Arch Phys Med Rehabil* **95**, 986-995 e1 (2014).
3. Rosenfeld, J.V. *et al.* Early management of severe traumatic brain injury. *Lancet* **380**, 1088-98 (2012).
4. Nieuwkamp, D.J. *et al.* Changes in case fatality of aneurysmal subarachnoid haemorrhage over time, according to age, sex, and region: a meta-analysis. *Lancet Neurol* **8**, 635-42 (2009).
5. Joy, M.T. *et al.* CCR5 Is a Therapeutic Target for Recovery after Stroke and Traumatic Brain Injury. *Cell* **176**, 1143-1157 e13 (2019).
6. Warner, D.S., James, M.L., Laskowitz, D.T. & Wijdicks, E.F. Translational research in acute central nervous system injury: lessons learned and the future. *JAMA Neurol* **71**, 1311-8 (2014).
7. Salehi, A., Zhang, J.H. & Obenaus, A. Response of the cerebral vasculature following traumatic brain injury. *J Cereb Blood Flow Metab* **37**, 2320-2339 (2017).
8. Alvarez-Sabin, J., Maisterra, O., Santamarina, E. & Kase, C.S. Factors influencing haemorrhagic transformation in ischaemic stroke. *Lancet Neurol* **12**, 689-705 (2013).
9. Kummer, T.T. *et al.* Experimental subarachnoid haemorrhage results in multifocal axonal injury. *Brain* **138**, 2608-18 (2015).
10. Wu, Y., Peng, J., Pang, J., Sun, X. & Jiang, Y. Potential mechanisms of white matter injury in the acute phase of experimental subarachnoid haemorrhage. *Brain* **140**, e36 (2017).
11. Yeo, L.L. *et al.* Timing of recanalization after intravenous thrombolysis and functional outcomes after acute ischemic stroke. *JAMA Neurol* **70**, 353-8 (2013).
12. Mokin, M., Rojas, H. & Levy, E.I. Randomized trials of endovascular therapy for stroke--impact on stroke care. *Nat Rev Neurol* **12**, 86-94 (2016).
13. Mendelson, S.J. & Prabhakaran, S. Diagnosis and Management of Transient Ischemic Attack and Acute Ischemic Stroke: A Review. *JAMA* **325**, 1088-1098 (2021).
14. Albers, G.W. *et al.* Thrombectomy for Stroke at 6 to 16 Hours with Selection by Perfusion Imaging. *N Engl J Med* **378**, 708-718 (2018).
15. Nogueira, R.G. *et al.* Thrombectomy 6 to 24 Hours after Stroke with a Mismatch between Deficit and Infarct. *N Engl J Med* **378**, 11-21 (2018).
16. Shah, F.A. *et al.* Pathological Comparisons of the Hippocampal Changes in the Transient and Permanent Middle Cerebral Artery Occlusion Rat Models. *Front Neurol* **10**, 1178 (2019).
17. Jassam, Y.N., Izzy, S., Whalen, M., McGavern, D.B. & El Khoury, J. Neuroimmunology of Traumatic Brain Injury: Time for a Paradigm Shift. *Neuron* **95**, 1246-1265 (2017).
18. Stocchetti, N. *et al.* Neuroprotection in acute brain injury: an up-to-date review. *Crit Care* **19**, 186 (2015).
19. Montaner, J. *et al.* Multilevel omics for the discovery of biomarkers and therapeutic targets for stroke. *Nat Rev Neurol* **16**, 247-264 (2020).
20. Childs, C. & Lunn, K.W. Clinical review: Brain-body temperature differences in adults with severe traumatic brain injury. *Crit Care* **17**, 222 (2013).

21. DeVience, S.J. *et al.* Metabolic imaging of energy metabolism in traumatic brain injury using hyperpolarized [1-(13)C]pyruvate. *Sci Rep* **7**, 1907 (2017).
22. Bramlett, H.M. & Dietrich, W.D. Pathophysiology of cerebral ischemia and brain trauma: similarities and differences. *J Cereb Blood Flow Metab* **24**, 133-50 (2004).
23. Sykes, G.P. *et al.* Aging Immune System in Acute Ischemic Stroke: A Transcriptomic Analysis. *Stroke* **52**, 1355-1361 (2021).
24. Willis, E.F. *et al.* Repopulating Microglia Promote Brain Repair in an IL-6-Dependent Manner. *Cell* **180**, 833-846 e16 (2020).
25. Lindblad, C. *et al.* Fluid proteomics of CSF and serum reveal important neuroinflammatory proteins in blood-brain barrier disruption and outcome prediction following severe traumatic brain injury: a prospective, observational study. *Crit Care* **25**, 103 (2021).
26. Banoei, M.M., Casault, C., Metwaly, S.M. & Winston, B.W. Metabolomics and Biomarker Discovery in Traumatic Brain Injury. *J Neurotrauma* **35**, 1831-1848 (2018).
27. Cao, F. *et al.* Apolipoprotein E-Mimetic COG1410 Reduces Acute Vasogenic Edema following Traumatic Brain Injury. *J Neurotrauma* **33**, 175-82 (2016).
28. Uhlmann, S. *et al.* Genome-Wide Analysis of the Circulating miRNome After Cerebral Ischemia Reveals a Reperfusion-Induced MicroRNA Cluster. *Stroke* **48**, 762-769 (2017).
29. Peng, J. *et al.* High-Throughput Sequencing and Co-Expression Network Analysis of lncRNAs and mRNAs in Early Brain Injury Following Experimental Subarachnoid Haemorrhage. *Sci Rep* **7**, 46577 (2017).
30. Zhong, J. *et al.* Altered expression of long non-coding RNA and mRNA in mouse cortex after traumatic brain injury. *Brain Res* **1646**, 589-600 (2016).
31. Buschmann, I.R., Busch, H.J., Mies, G. & Hossmann, K.A. Therapeutic induction of arteriogenesis in hypoperfused rat brain via granulocyte-macrophage colony-stimulating factor. *Circulation* **108**, 610-5 (2003).
32. Diprose, W.K. *et al.* Impact of Body Temperature Before and After Endovascular Thrombectomy for Large Vessel Occlusion Stroke. *Stroke* **51**, 1218-1225 (2020).
33. Huie, J.R. *et al.* Biomarkers for Traumatic Brain Injury: Data Standards and Statistical Considerations. *J Neurotrauma* (2020).
34. Morganti-Kossmann, M.C., Semple, B.D., Hellewell, S.C., Bye, N. & Ziebell, J.M. The complexity of neuroinflammation consequent to traumatic brain injury: from research evidence to potential treatments. *Acta Neuropathol* **137**, 731-755 (2019).
35. Longo, K.A. *et al.* Wnt10b inhibits development of white and brown adipose tissues. *J Biol Chem* **279**, 35503-9 (2004).
36. Li, L., Xiong, W.C. & Mei, L. Neuromuscular Junction Formation, Aging, and Disorders. *Annu Rev Physiol* **80**, 159-188 (2018).
37. Zetterberg, H. & Blennow, K. Fluid biomarkers for mild traumatic brain injury and related conditions. *Nat Rev Neurol* **12**, 563-74 (2016).
38. Lee, T.H. *et al.* Plasma ceramides are associated with outcomes in acute ischemic stroke patients. *J Formos Med Assoc* (2021).
39. Partoazar, A. *et al.* Neuroprotective phosphatidylserine liposomes alleviate depressive-like behavior related to stroke through neuroinflammation attenuation in the mouse hippocampus. *Psychopharmacology (Berl)* (2021).
40. Carney, N. *et al.* Guidelines for the Management of Severe Traumatic Brain Injury, Fourth Edition. *Neurosurgery* **80**, 6-15 (2017).

41. Powers, W.J. *et al.* Guidelines for the Early Management of Patients With Acute Ischemic Stroke: 2019 Update to the 2018 Guidelines for the Early Management of Acute Ischemic Stroke: A Guideline for Healthcare Professionals From the American Heart Association/American Stroke Association. *Stroke* **50**, e344-e418 (2019).
42. Reith, J. *et al.* Body temperature in acute stroke: relation to stroke severity, infarct size, mortality, and outcome. *Lancet* **347**, 422-5 (1996).
43. Deis, J.A. *et al.* Adipose Lipocalin 2 overexpression protects against age-related decline in thermogenic function of adipose tissue and metabolic deterioration. *Mol Metab* **24**, 18-29 (2019).
44. de Souza, C.A.P. *et al.* Melatonin multiple effects on brown adipose tissue molecular machinery. *J Pineal Res* **66**, e12549 (2019).
45. Gantner, M.L., Hazen, B.C., Conkright, J. & Kralli, A. GADD45gamma regulates the thermogenic capacity of brown adipose tissue. *Proc Natl Acad Sci U S A* **111**, 11870-5 (2014).
46. Weber, C. *et al.* Temperature-dependent sex determination is mediated by pSTAT3 repression of Kdm6b. *Science* **368**, 303-306 (2020).
47. Kano, O., Ikeda, K. & Iwasaki, Y. Do acute phase markers explain body temperature and brain temperature after ischemic stroke? *Neurology* **80**, 777-8 (2013).
48. Kloska, A., Malinowska, M., Gabig-Ciminska, M. & Jakobkiewicz-Banecka, J. Lipids and Lipid Mediators Associated with the Risk and Pathology of Ischemic Stroke. *Int J Mol Sci* **21**(2020).
49. Gafson, A.R. *et al.* Neurofilaments: neurobiological foundations for biomarker applications. *Brain* **143**, 1975-1998 (2020).
50. Hu, X. *et al.* Microglia/macrophage polarization dynamics reveal novel mechanism of injury expansion after focal cerebral ischemia. *Stroke* **43**, 3063-70 (2012).

Figure legends:

Fig.1 Transcriptome landscape of ABIs.

(A) Gene expression profile of differential expressed genes (DEGs) and associated functional term enrichment. Each column indicates a gene (top heatmap). The pie chart represents the gene counts of up-regulated (red), down-regulated (blue), and not-changed (white) genes in each acute brain injury model (top right pie plots). Gene members of key pathways enriched in each cluster (bottom heatmap) are shown.

(B) Heatmap showcasing dynamic profile of the genes in cluster 6 from Figure 1A. K-means was performed to split genes into 2 categories based on the gene expression in PM and TM models at 12H.

(C) The dynamically changed expression profile of the genes enriched in the four pathways displayed in Figure 1A of cluster 6 is constructed in this heatmap. The gene expression was transformed by z-score and then Hierarchical Clustering was performed. Each color represents the pathway which the gene enriched, consistent with pathways in cluster 6 from Figure 1A

(D) The expression distribution of genes in cluster 6 between PM and TM models at 12H is represented in this box plot. The line and box represent median and upper and lower quartiles ($*P < 0.05$, $**P < 0.01$, $***P < 0.001$).

(E) Scatterplot shows the correlation of NIHSS score with highest body temperature of transient acute ischemic stroke patients (TAIS) (yellow, R = 0.304, 95% confidence interval: 0.131 -

0.459, P = 0.0002, N = 41) and the correlation of NIHSS score with highest body temperature of permanent acute ischemic stroke patients (PAIS) (blue, R = 0.554, 95% confidence interval: 0.297 - 0.736, P = 0.0008, N = 119) during the first 72H of admission.

Fig.2 Proteomic characteristics of ABIs.

(A) The abundance profile of significantly changed proteins in the four acute brain injury models at 24H. Heatmap was calculated by Hierarchical Clustering analysis using union sets of significantly changed proteins in each group of acute brain injury model. K-means was used to split significantly changed proteins into 2 clusters at 24H.

(B) Simplified bar graphs are used to demonstrate the top 5 enriched GO terms of the significantly changed proteins related to the 2 clusters of four acute brain injury models at 24H.

(C) Scatter plots are used to represent the correlation between gene transcription level (mRNA) and translation level (Protein) of proteins enriched in pathways related to synaptic in cluster2 (Figure 2B bottom). The correlation coefficient and p values were calculated by the Pearson correlation method.

(D) A representative group of proteins in Figure 2C is used to show the dynamic protein change at three-time stages. The y axis represents log_2FC compare to control.

Fig.3 Co-variation of risk factors related to ABIs

(A) Pearson correlation coefficient distribution of the abundance of gene transcription level (mRNA) and translation level (Protein) in four acute brain injury models (SAH, TBI, PM, and TM) at three different time stages were calculated. The genes of each cluster were used in Figure 1A.

(B) A complete protein-protein interaction network (PPI) of the above-mentioned hub genes of each cluster from Figure 3A generated using Cytoscape. Genes labeled red represents hub genes and genes labeled gray represent genes that are related to hub genes.

(C) Pearson correlation coefficient distribution of hub genes in each acute brain injury model. The color of each sphere represents cluster number and the size of the sphere represents the absolute Pearson correlation coefficient value.

Fig.4 Metabolic and lipidomic characteristics of ABI models.

(A) The classification (left) the abundance (middle) of metabolites that significantly changed in the four acute brain injury models at 24H. Please refer to the methodology section for the classification criteria of metabolites. The bar plot on the right represents the number of metabolites in the form of positive and negative ions.

(B) The pie charts indicate the category of KEGG pathway enriched by differential metabolites in the four acute brain injury models at 12H, 24H, and 72H. The models are constructed from the inner layer to the outer layer are SAH, TBI, PM, and TM.

(C) The bar plot illustrates the number of significantly changed lipids in different classifications, which compared with the control group in four acute brain injury models at 24H.

(D) The Venn diagrams of significantly changed lipids for each acute brain injury model compared with the control group at 12H, 24H, and 72H.

Fig.5 Lipidome reveals a distinct pattern compared with transcriptome and proteome in PM and TM.

(A) Pie chart showing the fractions of related genes in different classes of lipids

(B) The joint proteomics and transcriptomics profile of TM and PM at three-time stages based on the related genes in five classes. The value in the heatmap represents the log2(fold change) compared with the control group.
(C) The abundance of significantly changed lipids in five classes from Figure 5A compared with the control group.

Extended Data Fig.1 The workflow of the ABI integrated omics study.
(A) Schematics of Acute Brain Injury research. The ipsilateral hemisphere (right) of acute brain injury mouse models, including 17 mice (N = 9 for transcriptomics analysis; N = 8 for proteomics, metabolomics, and lipidomics analysis). In each group at the three-time stages of SAH, TBI, PM, and TM, samples were obtained for proteomics, transcriptomics, metabolomics, and lipidomics analysis. The time stages for collecting brain samples were 12 hours (12H), 24 hours (24H), and 72 hours (72H) after the successful acute brain injury model construction.
(B) The stability and accuracy of all acute brain injury mouse models were verified by MRI assays before the integrated omics experiment process. Representative MRI-T2 images of the dorsal view of brains show the radiological characteristics of the ipsilateral hemisphere (right, R) and contralateral hemisphere (left, L) of acute brain injury models.
(C) Neurobehavioral tests including modified Garcia Score (for SAH), Neurological Severity Score (NSS, for TBI), as well as Neurological Score and Beam Walking (for PM and TM) were used to confirm the stability of the ABI models (***$P < 0.001$, compared to the control group).
(D) Statistics of the number of differential expressed genes in the ABI models compared with the control group at three-time stages. The pie charts above the bar plot indicate the proportion of DEGs that are up-or down-regulated.
(E) The scatter plot distribution of differential expressed genes between the ABI models at three different time stages and the control group. Red dots indicate genes that are up-regulated, and the blues indicate down-regulated genes. The values of the x-axis and y-axis represent the value (TPM) of gene expression after the logarithmic operation.

Extended Data Fig.2 Quality control of ABI mouse models and multi-omics data quality evaluation.
(A) Heatmaps showing the Pearson correlation coefficients of gene expression between biological repeats in four acute brain injury mouse models and control at different time stages.
(B) A statistical representation of the differential expressed genes number (DEGs) of the comparisons in four acute brain injury models at three-time stages.
(C) Heatmap demonstrating hierarchical clustering analysis of relative proteins, metabolites, and lipids abundances among four acute brain injury models in comparison to the control group at the three-time stages.
(D) Partial least squares-discrimination analysis (PLS-DA) reveals distinct characteristic patterns among different models based on their global proteome data at three-time stages.

Extended Data Fig.3 The dynamic changes of the proteins related to exocytosis in each ABI model at three-time stages.
(A) The correlation between gene transcription level (mRNA) and translation level (Protein) of proteins enriched in pathways related to exocytosis in category 1 (Figure 2B top). Correlation

coefficients and p values were calculated by the Pearson correlation method.

(B) A representative group of proteins in Figure S3A is used to show the dynamic protein change at three-time stages. The y axis represents log_2FC compare to control.

Extended Data Fig.4 The proteomics profiling in the ABI models at 12H and 72H.

The abundance profile of significantly changed proteins in the four acute brain injury models at 12H (A) and 72H (B). Heatmap was calculated by Hierarchical Clustering analysis using union sets of significantly changed proteins in each group of acute brain injury model. Simplified bar graphs are used to demonstrate the top 5 enriched GO terms of the significantly changed proteins related to the clusters of four acute brain injury models at 12H (C) and 72H (D).

Extended Data Fig.5 Hub genes analysis of ABI models.

(A) Cytohubba plugin of Cytoscape is used to screen the hub genes of the DEGs in each cluster. In the end, only the genes shared by the five methods were selected as the hub gene of each cluster. Circles of the Venn diagram represent the ways for the cytohubba plugin to identify the hub genes.

(B) The log_2FC changes in the transcription level (mRNA, top) and translation level (Protein, bottom) of hub genes relative to the control group at three-time stages.

Extended Data Fig.6 Metabolic characteristics of ABI models at 12H and 72H.

(A) The bar plot represents the number of differentially changed metabolites in the form of positive and negative ions among the four acute brain injury models at 12H and 72H.

(B) The classification (left) the abundance (right) of metabolites that significantly changed in the four acute brain injury models at 12H and 72H.

Extended Data Fig.7 Metabolic and lipidomic characteristics of ABI models.

The union of top 10 KEGG pathways in human disease (red text) and metabolism (blue text) in the four acute brain injury models at 12H (A), 24H (B), and 72H (C) according to the Venn diagram of Figure 4B (left, middle, right). (D) Bar plot showcasing the classification of significantly changed lipids of four acute brain injury models compared with the control at 12H and 72H.

Extended Data Fig.8 Different ABI models have different lipid regulatory factors.

The classification statistics of the significantly changed lipid molecules compared with the control group in each acute brain injury model at three-time stages.

Figures

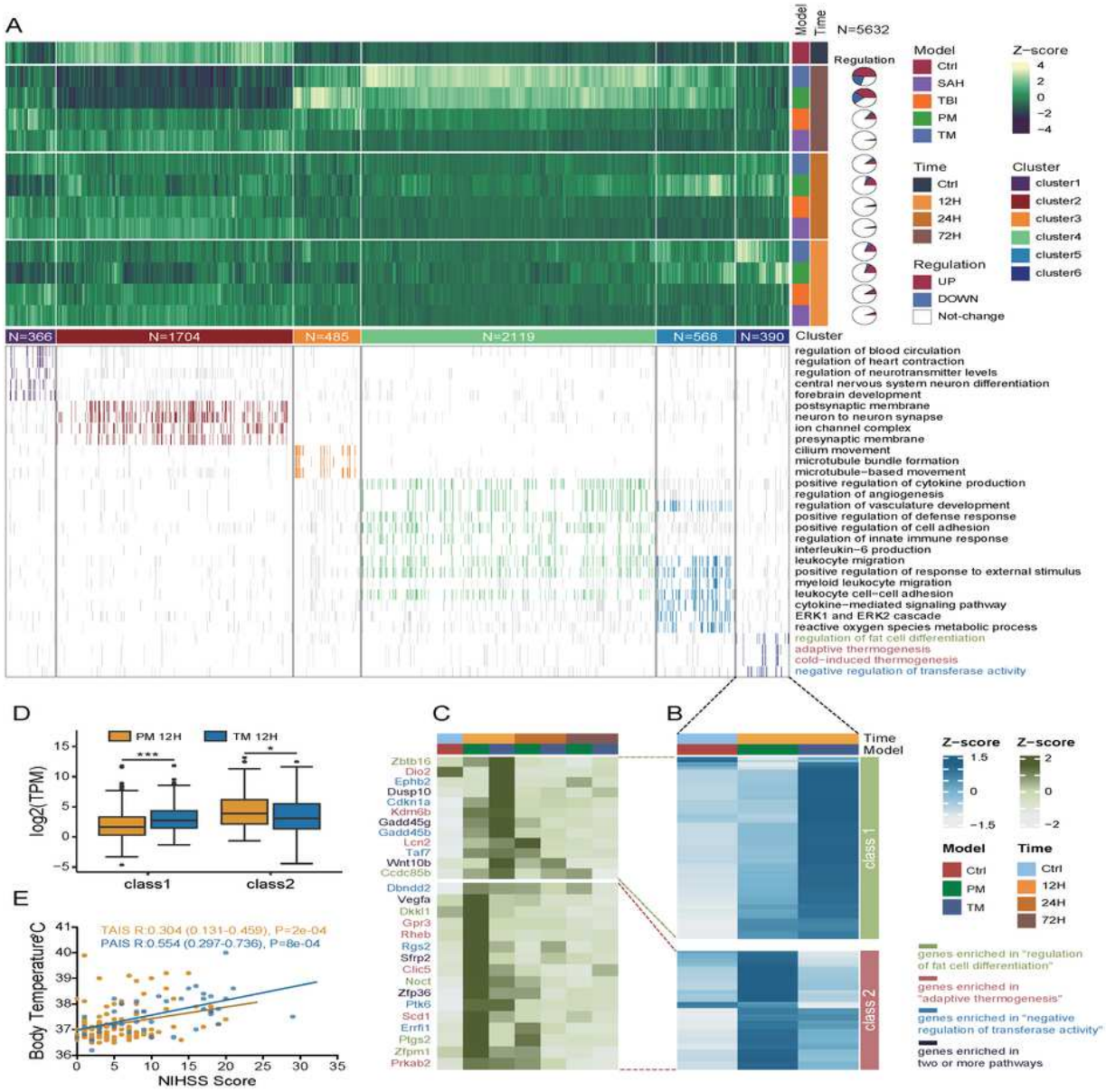

Figure 1

Transcriptome landscape of ABIs. Please see the Manuscript PDF file for the complete figure caption.

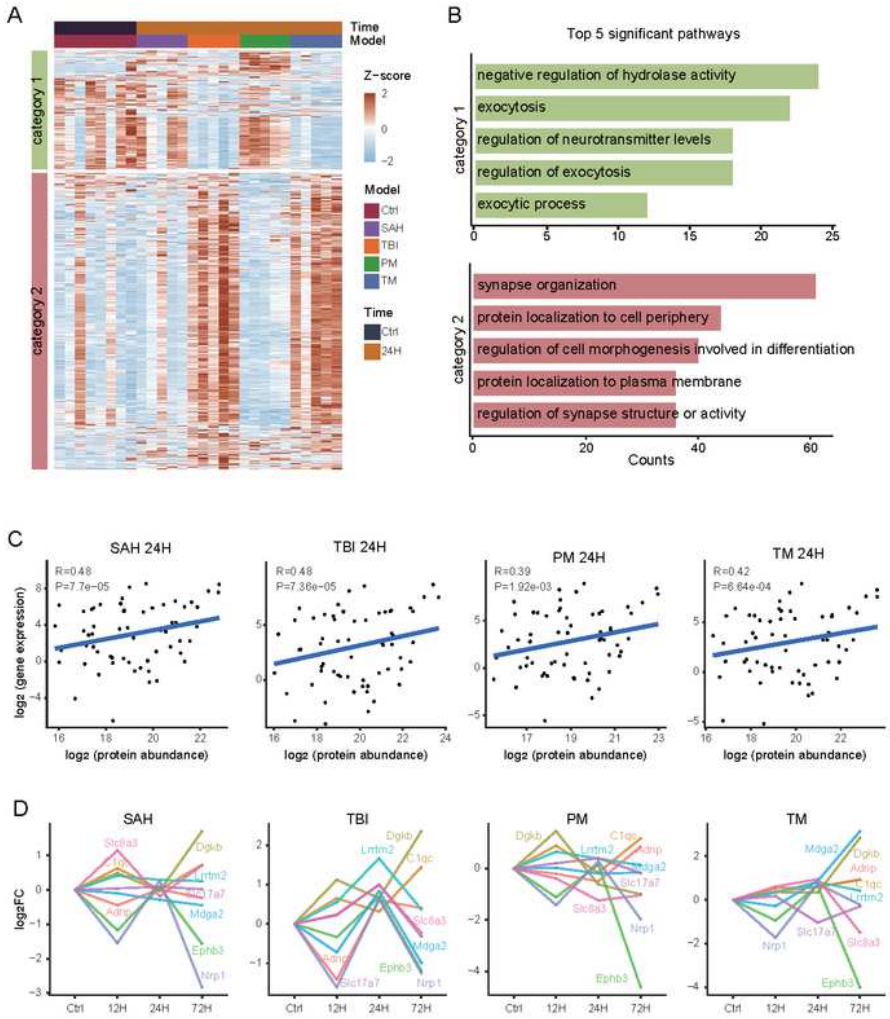

Figure 2

Proteomic characteristics of ABIs. Please see the Manuscript PDF file for the complete figure caption.

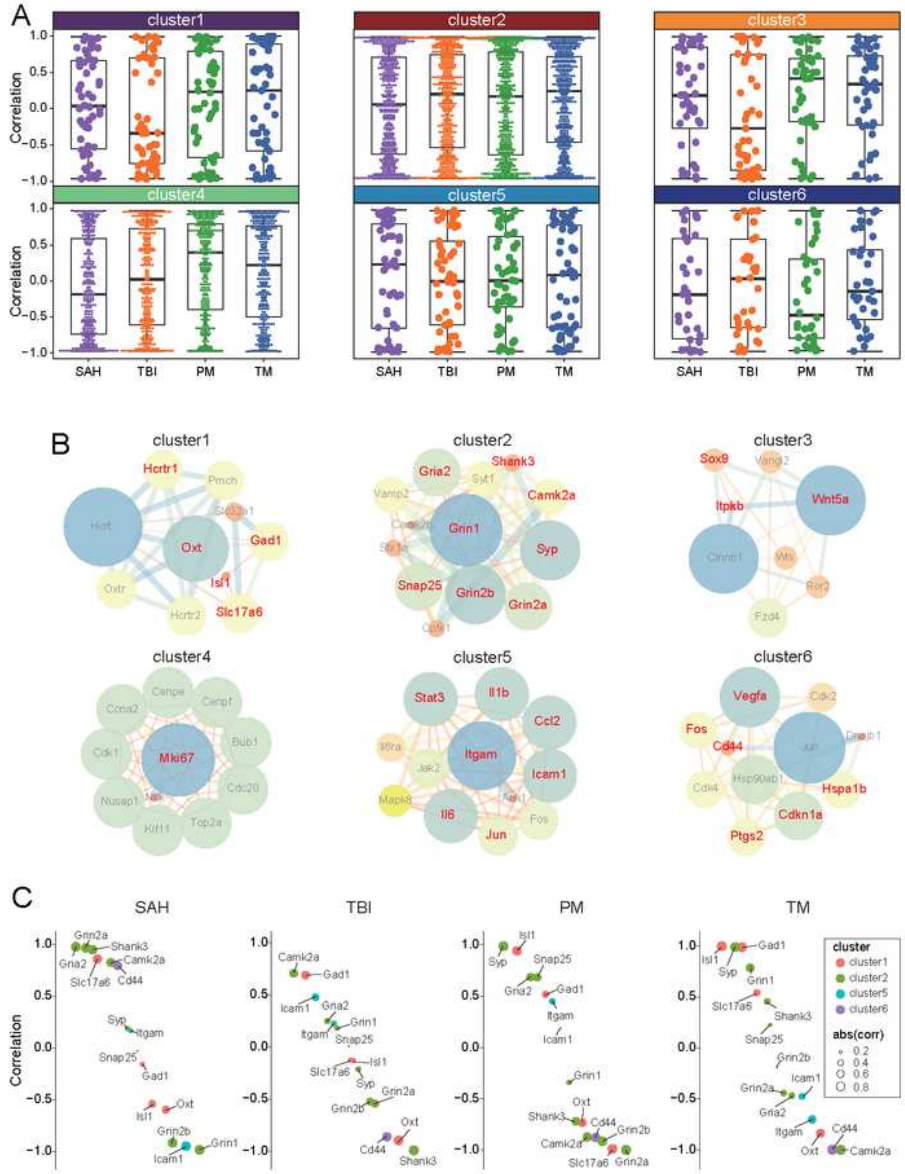

Figure 3

Co-variation of risk factors related to ABIs Please see the Manuscript PDF file for the complete figure caption.

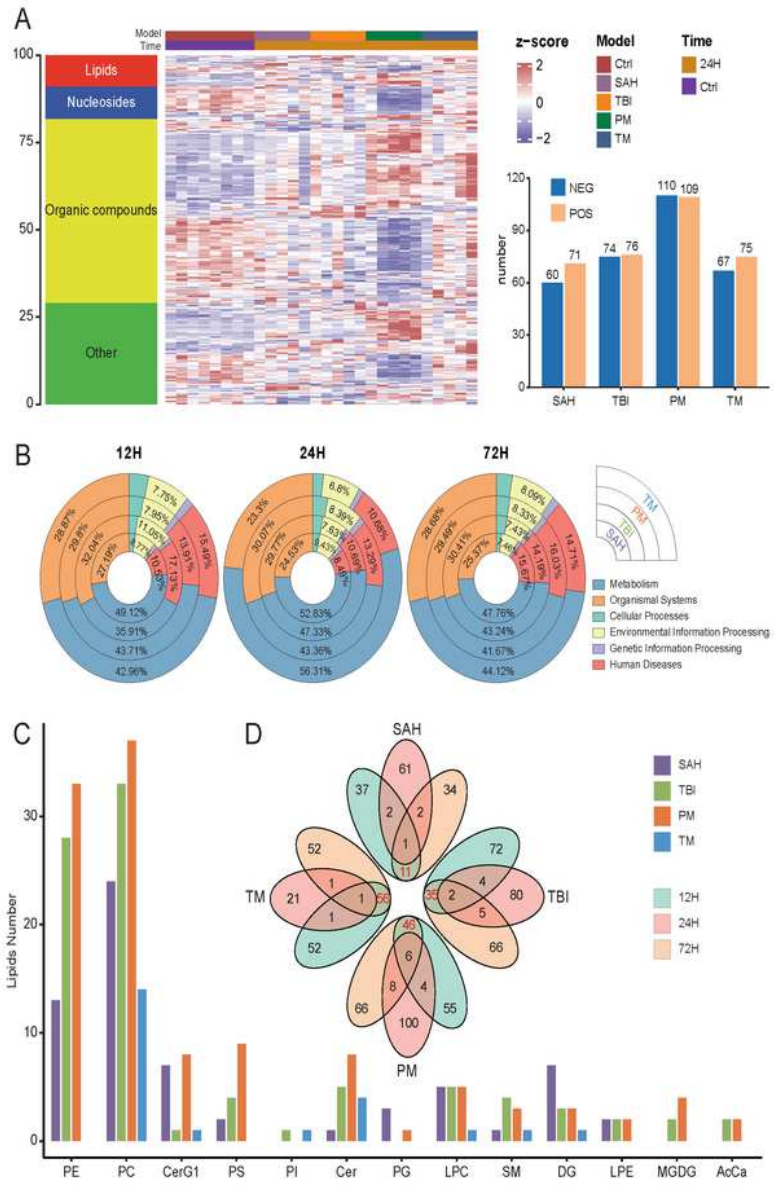

Figure 4

Metabolic and lipidomic characteristics of ABI models. Please see the Manuscript PDF file for the complete figure caption.

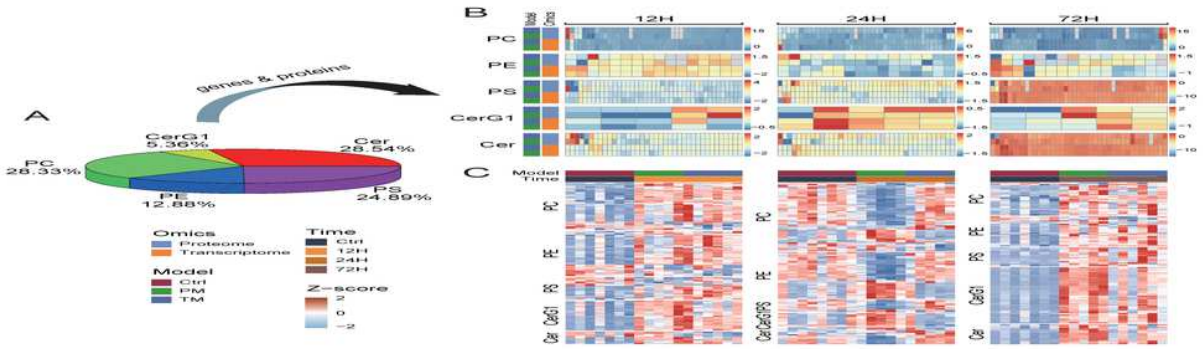

Figure 5

Lipidome reveals a distinct pattern compared with transcriptome and proteome in PM and TM. Please see the Manuscript PDF file for the complete figure caption.

Supplementary Files

This is a list of supplementary files associated with this preprint. Click to download.

- ExtendedDataFig.1.pdf
- ExtendedDataFig.2.pdf
- ExtendedDataFig.3.pdf
- ExtendedDataFig.4.pdf
- ExtendedDataFig.5.pdf
- ExtendedDataFig.6.pdf
- ExtendedDataFig.7.pdf
- ExtendedDataFig.8.pdf